Detuning related coupler kick variation of a superconducting nine-cell 1.3 GHz cavity

Thorsten Hellert* and Martin Dohlus
DESY, Notkestrasse 85, 22603 Hamburg, Germany
(Dated: November 22, 2017)

Superconducting TESLA-type cavities are widely used to accelerate electrons with long bunch trains, such has high repetition rate free electron lasers. The TESLA cavity is equipped with two higher order mode- and a fundamental power coupler (FPC), which break the axial symmetry of the cavity. The passing electrons therefore experience axially asymmetrical coupler kicks, that depend on the transverse beam position at the couplers and the RF phase. The resulting emittance dilution is studied in detail in literature. However, the kick induced by the FPC depends explicitly on the ratio of the forward and the backward traveling waves at the coupler, which has received little attention. The intention of this paper is to present the concept of discrete coupler kicks with a novel approach of separating the field disturbances related to the standing wave and a reflection dependent part. Particular attention is directed to the role of the penetration depth of the FPC antenna, thus the loaded quality factor of the cavity. The developed beam transport model is compared to dedicated experiments at FLASH and European XFEL. Both, the observed transverse coupling and detuning related coupler kick variations are in good agreement with the model. Finally, the expected trajectory variations due to coupler kick variations at European XFEL are investigated and results of numerical studies are presented.

I. INTRODUCTION

Single pass free electron lasers (FEL) are the state-of-the-art particle accelerators to generate high brilliance photon pulses [1]. At the FEL user facilities FLASH (Free-Electron Laser in Hamburg) [2, 3] and European XFEL (European X-Ray Free-Electron Laser) [4–6], the driving electron bunches are accelerated in superconducting radio-frequency (RF) resonators based on the TESLA (TeV-Energy Superconducting Linear Accelerator) [7] technology. The advantage of superconducting RF cavities is the ability to provide high bunch repetition rates.

The TESLA cavity is a 9-cell standing wave structure of about 1 m length whose fundamental transverse magnetic mode resonates at 1.3 GHz. It is equipped with two higher order mode (HOM) couplers at both ends of the cavity [8] in order to extract undesired field excitations. The fundamental power coupler (FPC) is installed horizontally at the downstream end of the cavity and connects the cavity to its power source.

Couplers break the axial symmetry of the cavity [9]. Their impact on the beam is illustrated in Figure 1, where tracking results are shown for a particle which enters the cavity on axis with an initial beam energy of 120 MeV. Plotted are the longitudinal (top), vertical (mid) and horizontal (bottom) momentum as a function of the longitudinal coordinate z. The significant change of transverse momenta at the coupler regions are referred to as coupler kicks. The sinusoidal dependence inside the cavity is related to axially symmetrical RF focussing [10], since the upstream HOM coupler kicks the beam off axis.

Coupler kicks depend on the RF phase and therefore distort different longitudinal slices of the beam by a different amount, which results in an increase of the projected emittance [11]. A large volume of published studies describe the effect of coupler kicks on emittance dilution [12–14] and its mitigation for different geometries of the superstructure [15–19]. However, the existing literature on coupler kicks largely ignores the role of different field configurations related to the forward and backward

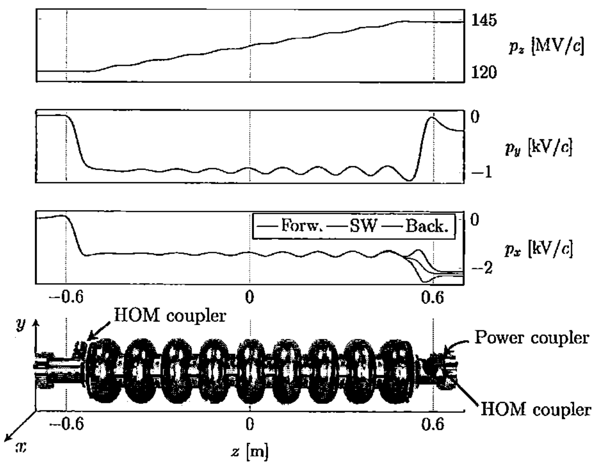

Figure 1. Tracking results for a particle which enters a TESLA cavity on axis with an initial beam energy of 120 MeV. Plotted are the longitudinal (top), vertical (mid) and horizontal (bottom) momentum as a function of the longitudinal coordinate z. The accelerating gradient is 24 MV m^{-1}. The significant change of transverse momenta at the coupler positions are related to coupler kicks. The sinusoidal variation inside the cavity is related to axially symmetrical RF focussing. Tracking is calculated for a purely forward traveling wave (red), a standing wave (blue) and a backward wave (black). Only the downstream horizontal coupler kick depends on the mode of cavity operation.

* thorsten.hellert@desy.de

traveling waves in the FPC. This work aims to close that gap.

Tracking in Figure 1 was done using different cavity field configurations, while the amplitude of the accelerating field is kept constant. The black color corresponds to a purely backward wave, thus a wave traveling from the cavity into the waveguide. The red color corresponds to the opposite, where the electromagnetic field is solely defined by the forward traveling wave from the waveguide into the cavity. The blue color corresponds to a standing wave, where both traveling waves have the same magnitude.

Figure 1 points out that the downstream coupler kick in the horizontal plane depends considerably on the reflection factor of the two traveling waves, whereas the energy gain and the vertical momentum is hardly affected. This is due to the fact that the FPC is mounted horizontally on the cavity and that the fields far away from the coupler are independent of the direction of the traveling waves.

The quality factor of the TESLA cavity is in the order of 10^{10} and wall losses can be neglected. In the absence of beam loading, the reflection factor is therefore determined by the detuning of the cavity. Due to the high quality factor, a small deformation, for example because of dynamic Lorentz forces [20] or microphonics [21], results in considerable detuning of the cavity. Variations of the detuning consequentially entail variations of coupler kicks.

The present study aims to explore the relationship between cavity detuning and coupler kicks. It provides a novel approach to quantify detuning related coupler kick variations by separating the impact of the standing and the traveling wave. Particular attention is furthermore given to the role of the penetration depth of the coaxial FPC antenna, thus the value of the loaded quality factor of the cavity.

A. Structure of this paper

This paper is organized in the following way: it begins with an introduction to the TESLA cavity and its couplers in Section II. Section III provides the mathematical principles to calculate general electromagnetic field configurations from a given field map. The main idea of discrete coupler kicks is developed in Section IV and quantified for different penetration depths of the FPC antenna in Section V. In Section VI we present the implementation of a linear beam dynamics model relying on discrete coupler kicks and proof its applicability by comparison with particle tracking. Comparison with dedicated experiments at FLASH and European XFEL is given in Section VII. Finally, the developed coupler kick model will be applied in Section VIII for beam dynamics simulations for European XFEL.

II. TESLA CAVITY

The TESLA cavity [7] is a 9-cell standing wave structure of about 1 m length whose lowest TM mode resonates at $f_0 = 1.3$ GHz. The cavity is built from solid niobium and is cooled by superfluid helium at 2 K. The fundamental advantage of superconducting cavities as compared to normal conducting cavities is the low surface resistance of about 10 nΩ at 2 K. This allows for high wall currents with little heat losses. The quality factor Q_0 of a cavity is defined as the ratio of the energy stored in the cavity U to the energy dissipated in the cavity walls P_{diss} per RF cycle,

$$Q_0 = \frac{2\pi f_0 U}{P_{\text{diss}}}, \tag{1}$$

which corresponds to the ratio of the resonance frequency to the width of the resonance curve. The typical quality factors of normal conducting cavities are in the range of 10^4 - 10^5 while for TESLA cavities $Q_0 > 10^{10}$. A schematic drawing of a TESLA cavity is shown in Figure 2.

The bunched electron beam excites eigenmodes of a variety of frequencies in the cavity. If the frequency of the regarded mode exceeds the resonance frequency of the fundamental mode, it is called higher order mode (HOM). Due to the high quality factor, the damping time constants of these modes are large compared to the typical bunch spacing. In order to prevent multi-bunch instabilities and beam breakup [22, 23], additional measures to damp HOMs have to be taken. For this reason two HOM-couplers [8] are mounted at both ends of the cavity in order to extract undesired field excitation. A 1.3 GHz notch filter is incorporated to prevent energy extraction from the fundamental mode. Upstream and downstream HOM coupler are oriented at 115 ° with respect to each other, as can be seen in Figure 3. The geometry of the HOM coupler and its resulting impact on the beam does not vary between FLASH and European XFEL.

The fundamental power coupler (FPC) has to carry out the transition of the high power RF from a warm, air-filled waveguide system through a coaxial connection into the cold cavity. The amount of power coupled from the waveguide into the cavity and vice versa is characterized by the external quality factor Q_{ext} of the cavity.

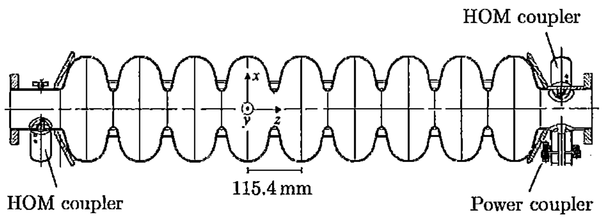

Figure 2. Longitudinal cross-section of a TESLA cavity. The beam direction is from left to right, thus the fundamental power coupler is located at the downstream end of the cavity.

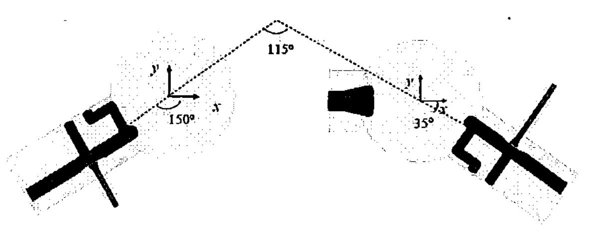

Figure 3. Geometry and orientation of the higher order mode (HOM, upstream and downstream) and fundamental power coupler (FPC, downstream).

The loaded quality factor Q_L characterizes both, the wall losses and the external power losses through the coupler and follows from Eq. (1) as

$$\frac{1}{Q_L} = \frac{1}{Q_{\text{ext}}} + \frac{1}{Q_0}, \tag{2}$$

while for superconducting cavities $Q_{\text{ext}} \ll Q_0$. The loaded quality factor is therefore determined by the external losses through the coupler. Different coupler specializations were developed [24] in order to account for different operational conditions.

Figure 4 shows a simplified schematic of the TTF-3 power coupler used at FLASH and European XFEL. It is based on the International Linear Collider (ILC) [25] design and optimized for a pulsed RF operation with high accelerating gradients and a duty cycle of about 1 %. The RF input power is about 200 kW. By moving the inner conductor of the coaxial line in a range of 10 mm, the loaded quality factor Q_L can be varied in the nominal range $10^6 - 10^7$ to allow not only for different beam loading conditions [26], but also to facilitate an in-situ high power processing of the cavities [27]. The cavity bandwidth at the typical value of $Q_L = 3 \times 10^6$ at FLASH is about 430 Hz. European XFEL operates at $Q_L = 4.6 \times 10^6$ with a resulting bandwidth of about 280 Hz.

At FLASH and European XFEL, a 1.3 GHz TESLA cavity based injector module accelerates the beam off crest in order to impose an energy chirp along the bunch for the needs of further longitudinal bunch compression. A following third harmonic system, operating at 3.9 GHz, decelerates the beam and thereby linearizes the longitudinal phase space of the bunches.

The 3.9 GHz cavity [28, 29] design is similar to a scaled version of the 1.3 GHz TESLA cavity. An alternate coupler orientation for each second cavity is used to compensate the coupler kick partially. At FLASH each second cavity is rotated by 180° around the y-axis [30], see Figure 5. The European XFEL uses a rotation of 180° around the z-axis [31], which leads to a cancellation of the offset independent part of the coupler kick.

The power coupler antenna position of the 3.9 GHz cavity is fixed. In order to change Q_L, a 3-stub tuner is installed in the waveguides. The cavity geometry in the proximity of the beam does therefore not vary for different Q_L.

III. FIELD CALCULATIONS

In order to investigate coupler kicks numerically, precise knowledge of the electromagnetic fields is required. This section provides the mathematical principles which are needed to generalize the field configuration from a given traveling wave field map.

The time harmonic field in a perfect electric conducting cavity that is equipped with couplers can be written as:

$$\begin{aligned}
\vec{E}(\vec{r}, t) &= \Re\left\{\vec{\mathbf{E}}(\vec{r}) \cdot \exp^{i\omega t}\right\} \\
\vec{B}(\vec{r}, t) &= \Re\left\{\vec{\mathbf{B}}(\vec{r}) \cdot \exp^{i\omega t}\right\} \\
\vec{\mathbf{E}}(\vec{r}) &= A_f e^{i\phi_f} \vec{\mathbf{E}}_0(\vec{r}) + A_b e^{i\phi_b} \vec{\mathbf{E}}_0^*(\vec{r}) \\
\vec{\mathbf{B}}(\vec{r}) &= A_f e^{i\phi_f} \vec{\mathbf{B}}_0(\vec{r}) - A_b e^{i\phi_b} \vec{\mathbf{B}}_0^*(\vec{r}).
\end{aligned} \tag{3}$$

$A_{[f/b]}$ and $\phi_{[f/b]}$ are the amplitude and phase of the forward and backward traveling wave to/from the power coupler, respectively, ω the frequency of excitation and $\vec{\mathbf{E}}_0$, $\vec{\mathbf{B}}_0$ the forward solution for the electric and magnetic field component of the excited mode. The bold letters indicate complex values.

A standing wave field is stimulated if $|A_b| = |A_f|$. Ignoring wall losses this condition is fulfilled in absence of a beam current and can be easily realized for EM field calculation either with port stimulation or by an eigenmode solver [15].

$|A_b| \neq |A_f|$ corresponds to a net-energy-flow from/to the cavity. As long as wall losses are neglected this is the case if the stored energy in the cavity is changed, for example while filling the cavity, or through beam loading. In order to account for an energy flow, a traveling wave

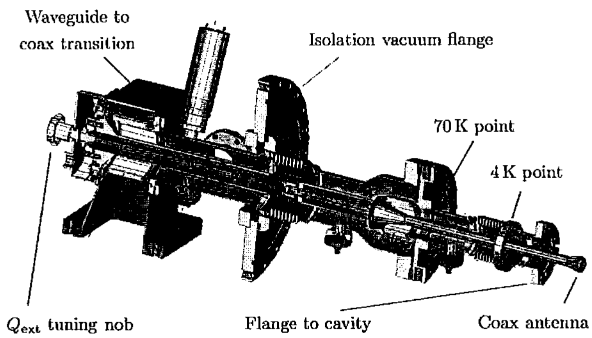

Figure 4. Schematic drawing of the TTF-3 fundamental power coupler of the TESLA cavity. The waveguide (lower left end) connects the cavity with the RF power source and is at room temperature. A remote controlled stepper motor allows to move the position of the coaxial antenna in the cavity beam pipe (right end).

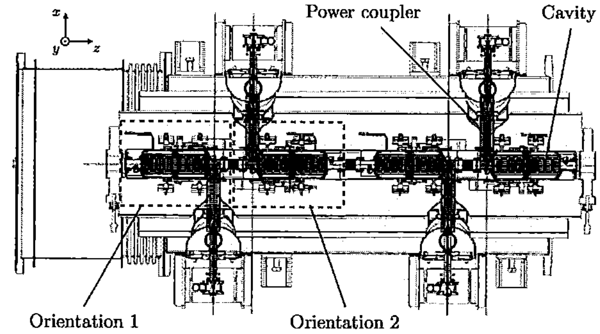

Figure 5. Schematic drawing of the third harmonic module at FLASH. Four cavities with alternate coupler orientation with respect to the beamline are installed in one cryomodule.

is required which implies a field with linear independent real- and imaginary-part.

To get a second and linear independent solution, the field excitation by the beam current has to be considered. There are at least three other approaches (without beam excitation): 1) the power transfer to the beam is replaced by wall losses, 2) the standing wave solution at a different frequency ω_2 is used (with $|\omega_2 - \omega| \ll \omega/Q_L$) and 3) a decaying eigensolution is calculated. Approach 1) needs a (driven) frequency domain solver with surface losses. Approach 2) needs a frequency domain solver without losses (perfect conducting boundary) or a loss-free eigenmode solver with two different cavity geometries (lengths of the FPC waveguide). Approach 3) needs a complex eigenmode solver with waveguide boundaries.

The 3D field map provided by Ref. [32] utilizes the latter approach. It describes the cavity fundamental mode including the fields induced by both higher order mode (HOM) and the fundamental power coupler (FPC). There are different field maps available in Ref. [33], which are calculated for different penetration depths of the coaxial antenna of the FPC. This reflects different values of the loaded quality factor of the cavity.

The field maps are given as a table of sine- and cosine-like amplitudes, $\vec{E}_b^{sin}(\vec{r})$ and $\vec{E}_b^{cos}(\vec{r})$, respectively for a decaying eigenmode with a backward traveling wave from the cavity into the waveguide.

In general the normalization of eigensolutions is arbitrary in amplitude and phase. For convenience we suppose a phase-normalization such that the electric field energy is maximal at $t = 0$. Therefore the $\vec{E}_b^{cos}$ part describes the main field that accelerates the particles while the weak $\vec{E}_b^{sin}$ field is unavoidable for a power flow (averaged over one period of time). The origin of the z-coordinate can be chosen so that the integrated longitudinal field, observed by a particle with $z = ct$, is maximal. This is approximately the case for an origin in the middle of a cell and in particular for an origin in the middle of a 9-cell cavity.

Under the stated preconditions, the electric field of the backward wave, $\vec{E}_b(\vec{r},t)$, has the following spatiotemporal dependency

$$\vec{E}_b(\vec{r},t) = \vec{E}_b^{cos}(\vec{r})\cos(\omega t) + \vec{E}_b^{sin}(\vec{r})\sin(\omega t)\,, \qquad (4)$$

with ω being the angular frequency of the mode. Using the Maxwell equations, the electric field of the forward wave $\vec{E}_f(\vec{r},t)$ can be calculated by reversing time as

$$\vec{E}_f(\vec{r},t) = \vec{E}_b^{cos}(\vec{r})\cos(\omega t) - \vec{E}_b^{sin}(\vec{r})\sin(\omega t)\,. \qquad (5)$$

The overall electric field component for the general case with a given accelerating voltage V_0 and phase ϕ with respect to the beam can then be calculated as

$$\vec{E}(\vec{r},t) = \Re\left[V_0/V_n\, e^{i(\omega t+\phi)} \cdot \left(\vec{E}_b^{cos}(\vec{r}) + i\,\mathbf{\Gamma}\cdot\vec{E}_b^{sin}(\vec{r})\right)\right]\,, \qquad (6)$$

where V_n normalizes the field to the Eigenmode solution of the field map. For the proposed convenient phase-normalization and origin of the z coordinate V_n is a real number. The parameter

$$\mathbf{\Gamma} = (A_b e^{i\phi_b} - A_f e^{i\phi_f})/(A_b e^{i\phi_b} + A_f e^{i\phi_f})\,, \qquad (7)$$

describes the ratio between the sum and difference of forward and backward waves in a particular reference plane and corresponds to the negative normalized admitance. The reference plane is chosen to be at a field-node for on-resonance-SW-operation. This is a position that is approximately a multiple of $\lambda/2$ from the tip of the coupler antenna, where λ is the RF wavelength. For this choice of reference plane the sum of forward and backward waves (or the denominator of Eq. (7)) is directly proportional to the amplitude of the accelerating field.

Due to the high quality factor of the TESLA cavity wall losses can be neglected. $\mathbf{\Gamma}$ is therefore determined by the amount of beam loading and the detuning of the cavity.

The magnetic field behaves analogously, using similar symmetry properties of the field components, $\vec{B}_f(\vec{r},t) = -\vec{B}_b(\vec{r},-t)$, and follows as

$$\vec{B}(\vec{r},t) = \Re\left[V_0/V_n\, e^{i(\omega t+\phi)} \cdot \left(\mathbf{\Gamma}\cdot\vec{B}_b^{cos}(\vec{r}) + i\,\vec{B}_b^{sin}(\vec{r})\right)\right] \qquad (8)$$

Please note that beam loading induces a backward traveling wave which is not included in Eqs. (6, 8).

IV. DISCRETE COUPLER KICKS

A charged particle which traverses the cavity with a given electric and magnetic field configuration on a trajectory with speed $\vec{v}$ at any time t experiences an external Lorentz force

$$\vec{F}(\vec{r},t) = q\left[\vec{E}(\vec{r},t) + \vec{v}(t)\times\vec{B}(\vec{r},t)\right] = q\,\vec{V}'(\vec{r},t) \qquad (9)$$

where $\vec{V}$ is the effective voltage experienced by the particle. It is plotted in Figure 6 for an ultra-relativistic particle which traverses the TESLA cavity on axis with the

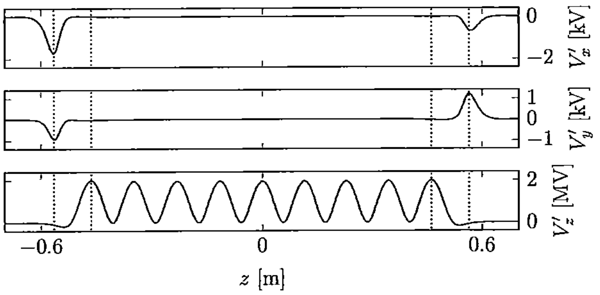

Figure 6. Horizontal (top), vertical (mid) and longitudinal (bottom) voltage as experienced by an ultra-relativistic charged particle which traverses the cavity on axis.

speed of light ($\vec{v}(t) = c\,\vec{e}_z$) as a function of the longitudinal coordinate z. The lower row indicates the nine-cell geometry of the cavity. The two upper rows point out the influence of the field disturbances caused by the upstream and downstream coupler region, since the particle trajectory is evaluated on axis where the fundamental mode has no transverse components.

The main idea behind discrete coupler kicks (DCK) [12] is to describe the impact of the transverse forces induced by the couplers onto the particle by a discrete kick at the coupler position. The axially symmetrical RF focusing [10] can then be accounted for by using the 2D transfer matrix of the cavity.

The integrated transverse field strength affecting an ultra-relativistic paraxial particle is given by

$$\mathbf{V}_\perp(x,y) = \int dz \left[\vec{\mathbf{E}}_\perp(\vec{r}) + c\,\vec{e}_z \times \vec{\mathbf{B}}(\vec{r})\right] e^{i\frac{\omega z}{c}} \qquad (10)$$

and can be easily separated for the upstream and downstream coupler region for on-axis trajectories by evaluating the integral from/to the center of the cavity to/from infinity. However, if Eq. (10) is evaluated that way for any $x \neq 0, y \neq 0$, the offset-dependent edge focusing of the cavity fundamental mode is not compensated and the calculated voltage is not purely induced by the couplers. In order to isolate the integrated transverse fields induced by the couplers

$$\mathbf{V}_\mathrm{c}(x,y) = \mathbf{V}_\perp(x,y) - \mathbf{V}_\mathrm{RZ}(r) \qquad (11)$$

for any $x \neq 0, y \neq 0$, the axially symmetrical RF focussing part of the field, $\mathbf{V}_\mathrm{RZ}$, has to be removed. This can be done by using the 3D field map of the TESLA cavity and extracting the monopole part, for example by averaging the field map over different azimuthal rotations around the cavity axis.

The real part of $\mathbf{V}_\mathrm{c}$ corresponds to a net deflection of the bunch centroid, whereas the imaginary part represents a kick which depends on the phase-offset $\Delta\phi = \omega\,\Delta t$ due to a time offset Δt of the individual particle with respect to the reference particle. This time-dependent kick induced by the couplers distorts different longitudinal slices of the beam by a different amount, which results in an increase of the projected emittance [11].

The transverse RF kick is the integrated transverse momentum change relative to the longitudinal momentum of the beam. This kick $\vec{k} = [x', y']$, induced by a coupler, can therefore be calculated as

$$\vec{k}(x,y) = \frac{e\,V_0}{E_0} \Re\left\{\tilde{\mathbf{V}}(x,y)\cdot e^{i\phi}\right\} \qquad (12)$$

with E_0 being the beam energy at the corresponding coupler region, V_0 and ϕ the amplitude and phase of the accelerating field, respectively, e the elementary charge and x and y the transverse beam position at the coupler location. $\tilde{\mathbf{V}}$ is the normalized complex kick factor, defined as

$$\tilde{\mathbf{V}}(x,y) = \frac{\mathbf{V}_c(x,y)}{\mathbf{V}_\parallel} \qquad (13)$$

with

$$\mathbf{V}_\parallel = \int dz\,\vec{e}_z \cdot \vec{\mathbf{E}}(0,0,z)\,e^{i\frac{\omega z}{c}} \qquad (14)$$

and holds the information of the axially asymmetrical field disturbances induced by the couplers. By taking the field map Eqs. (6, 8) into account, the normalized complex kick factor for the general case of an arbitrary $\mathbf{\Gamma}$ can be written as

$$\tilde{\mathbf{V}}(x,y) = \frac{1-\mathbf{\Gamma}}{2}\tilde{\mathbf{V}}^b(x,y) + \frac{1+\mathbf{\Gamma}}{2}\tilde{\mathbf{V}}^f(x,y) \qquad (15)$$

where $\tilde{\mathbf{V}}^b$ and $\tilde{\mathbf{V}}^f$ hold the field disturbances caused by backward and forward traveling wave, respectively. $\tilde{\mathbf{V}}^b$ and $\tilde{\mathbf{V}}^f$ can be calculated directly from a field map, using Eqs. (6, 8) by setting $V_0/V_n = 1$, $\phi = 0$ and $\Gamma = \pm 1$.

From Eq. (15) directly follows, that $\tilde{\mathbf{V}}$ can be separated in a standing wave part and a reflection dependent part as

$$\tilde{\mathbf{V}}(x,y) = \frac{1}{2}\,\tilde{\mathbf{V}}^\mathrm{SW}(x,y) + \frac{\mathbf{\Gamma}}{2}\,\tilde{\mathbf{V}}^\mathrm{R}(x,y)\,, \qquad (16)$$

where $\tilde{\mathbf{V}}^\mathrm{SW} = \tilde{\mathbf{V}}^f + \tilde{\mathbf{V}}^b$ and $\tilde{\mathbf{V}}^\mathrm{R} = \tilde{\mathbf{V}}^f - \tilde{\mathbf{V}}^b$ hold the field disturbances caused by the sum and the difference of the forward and backward traveling waves, respectively. Only the fields related to the reflection dependent part depend on the parameter $\mathbf{\Gamma}$.

The real and imaginary parts of the normalized complex kick factor $\tilde{\mathbf{V}}(x,y)$ as defined in Eq. (16) is plotted in Figure 7 for both, the upstream and the downstream coupler region for different transverse beam positions x and y. Different $\mathbf{\Gamma}$, thus modes of cavity operation, are evaluated using a field map with an antenna penetration depth of 8 mm. All vectors are scaled by the same amount in order to assure a qualitative comparison.

For the TESLA cavity, the kicks caused by the HOM couplers have the same order of magnitude as that from

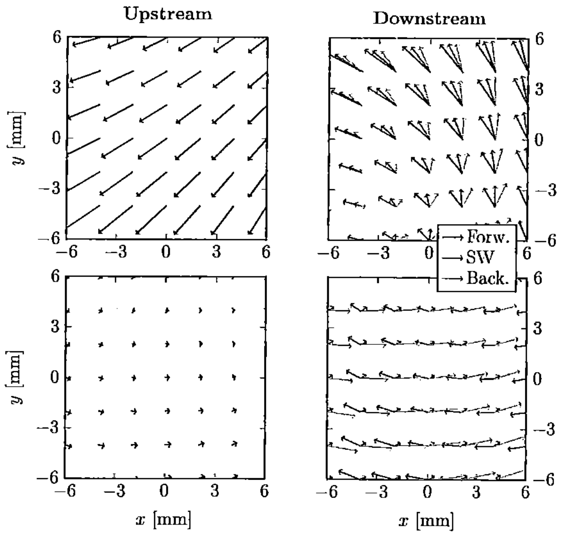

Figure 7. Real (upper row) and imaginary part (lower row) of the normalized complex kick factor for the upstream (left) and downstream coupler region (right) as a function of the transverse coordinates x and y. All vectors are scaled by the same amount in order to assure a quantitative comparison. The three colors in the right correspond to the case of pure forward traveling wave (blue) in the cavity, e.g. no backward wave and $\mathbf{\Gamma} = -1$, standing-wave operation (red, $\mathbf{\Gamma} = 0$) and pure backward traveling wave (yellow, $\mathbf{\Gamma} = 1$). Note that the kick induced by HOM couplers does not change for different $\mathbf{\Gamma}$. The net effect of the FPC is primarily horizontal.

the power coupler. The kick induced by the upstream HOM coupler does not depend on $\mathbf{\Gamma}$, as already indicated in Figure 1. This is due to the fact that the electromagnetic field away from the fundamental power coupler is, to a very good approximation, described by a standing wave and is not affected by the ratio of the forward and backward traveling wave. The static part of the downstream kick with respect to different $\mathbf{\Gamma}$ relates to the downstream HOM coupler. The $\mathbf{\Gamma}$-dependent part relates to the fundamental power coupler, which primarily acts horizontally. Coupler kicks of the FPC can therefore respond partially independent from the resonating accelerating field to variations of the forward and backward traveling wave.

V. NORMALIZED COUPLER KICK COEFFICIENTS

In this section we quantify coupler kicks for different FPC configurations by analyzing the normalized coupler kick coefficients.

It is reasonable to linearize the normalized complex kick factor $\tilde{\mathbf{V}}(x,y)$ around the cavity axis. The zeroth and first order kick $\vec{k}$ on a bunch induced by a coupler as defined in Eq. (12) can therefore be expressed as

$$\vec{k}(x,y) \approx \frac{eV_0}{E_0} \cdot \Re\left\{\left[\begin{pmatrix} V_{0x} \\ V_{0y} \end{pmatrix} + \begin{pmatrix} V_{xx} & V_{xy} \\ V_{yx} & V_{yy} \end{pmatrix} \cdot \begin{pmatrix} x \\ y \end{pmatrix}\right] e^{i\phi}\right\}, \tag{17}$$

where x and y are the bunch horizontal and vertical offset at the coupler position. From the Maxwell equations follows that $V_{yy} = -V_{xx}$ and $V_{xy} = V_{yx}$. Thus, coupler kicks are up to first order well described with four normalized coupler kick coefficients $[V_{0x}, V_{0y}, V_{xx}, V_{xy}]$.

As described earlier, the field maps available in Ref. [33] for the ILC style cavity are calculated for different penetration depths $d = [0, 2, 4, 6, 8, 10]$ mm of the coaxial antenna of the fundamental power coupler. The corresponding values for the loaded quality factor are $Q_L = [12.61, 8.30, 5.57, 3.81, 2.67, 1.91] \times 10^6$. The normalized coupler kick coefficients $[V_{0x}, V_{0y}, V_{xx}, V_{xy}]$ are calculated for $\tilde{\mathbf{V}}^{\mathrm{SW}}$ and $\tilde{\mathbf{V}}^{\mathrm{R}}$ for the upstream and downstream coupler region with different field maps, thus different values for the loaded quality factor Q_L. The coefficients are listed in Tables I, II and III in the Appendix.

The fields at the upstream coupler are, to a very good approximation, independent of the position of the coupler antenna. However, the impact of the downstream couplers on the transverse beam dynamics is significantly affected by the coupler antenna position.

The Q_L-dependence is shown in Figure 8 for the standing wave and the reflection dependent part in the left and right column, respectively. The coupler kick is about five orders of magnitude smaller than the longitudinal kick. The vertical coefficients V_{0y} and V_{xy} for both waves are insensitive to the antenna position, as it is expected from the geometry. Furthermore they are zero for the traveling wave. However, the horizontal coefficients related to the standing wave depend on the antenna position. Thus, for a given $\mathbf{\Gamma}$ the overall downstream coupler kick increases with higher Q_L.

The magnitude of the reflection dependent coefficients decreases with higher Q_L. This is due to the fact that the transition region in which the traveling wave into the coax changes to a standing wave in the cavity is smaller for larger Q_L [18]. Thus, for very high Q_L values the waves excited on the cavity axis will be standing waves, even in the coupler region.

Real and imaginary parts of most coefficients differ significantly from each other. A variation of the cavity phase will result in coupler kick variations. The imaginary parts of the reflection dependent coefficients exceed the real parts. Therefore, detuning related coupler kick variations are stronger in cavities which are operated off crest, as follows from Eq. (17).

The standard Q_L setting at FLASH is 3.1×10^6 whereas it is 4.6×10^6 at European XFEL. Both Q_L settings are not exactly represented by the field maps. Within the investigated range the Q_L-dependence of coupler kicks is considerable. An appropriate beam dynamics model relying on discrete coupler kicks should therefore use precise coupler kick coefficients. The Q_L-dependence of the normalized coupler kick coefficients V_{ij} is well described as

$$V_{ij} = 10^{-6}\left[c_1 + \frac{c_2}{Q_L/10^6 + c_3} + i\left(c_4 + \frac{c_5}{Q_L/10^6 + c_6}\right)\right] \quad (18)$$

with c_i being fit parameters for each coefficient. The dashed lines in Figure 8 indicate the solutions of Eq. (18) with the fit parameters listed in Tables IV and V in the Appendix.

The presented coupler kick model allows for a rough estimation regarding detuning related coupler kick variation. From the RF Eqs. (26) it follows that for a given accelerating gradient and beam current, the variation $\Delta\mathbf{\Gamma}$ and the detuning Δf are related according to

$$\Delta\mathbf{\Gamma}(\Delta f) = i\,\frac{2\,Q_L}{f_0}\cdot\Delta f \quad (19)$$

The horizontal zeroth order coupler kick variation which is related to the reflection dependent part is then given by

$$\Delta k_x^0 = \frac{e\,V_0}{E_0}\Re\{\frac{\Delta\mathbf{\Gamma}}{2}\cdot V_{0x}^{\mathrm{R}}\cdot e^{i\phi}\} \quad (20)$$

Thus, for the typical $Q_L = 3\times10^6$ and $\phi = 0°$ at FLASH it follows that

$$\Delta k_x^0 = -\frac{e\,V_0}{E_0}\,0.177\,\mathrm{\mu rad\,Hz^{-1}} \quad (21)$$

which results, for example, in a coupler kick variation of about 3.5 µrad for a cavity with $V_0 = 20\,\mathrm{MV}$, initial beam energy of $E_0 = 100\,\mathrm{MeV}$ and a detuning of $\Delta f = 100\,\mathrm{Hz}$.

The normalized coupler kick coefficients for the 3.9 GHz cavity are calculated analogously from the field map available at Ref. [34]. The values for orientation 1 (cf. Fig. 5) are listed in Table I.

VI. IMPLEMENTATION OF COUPLER KICKS IN LINEAR BEAM DYNAMICS MODEL

In this section the implementation of discrete coupler kicks into a linear beam dynamics model is presented, its accuracy for different beam energy is investigated and tracking with ASTRA [35] is used as reference.

Considering linear beam dynamics, the change of transverse coordinates can be written in terms of a matrix formalism as $\vec{u}_1 = M\cdot\vec{u}_0$,with $\vec{u}_1$ and $\vec{u}_0$ holding the particle transverse input and output coordinates $\vec{u}_i = [x, x', y, y']_i$, respectively, and M being the transfer matrix. The transfer matrix of an axially symmetrical RF cavity is given by Ref. [36] and can be found in Eq. (24) in Section XI A in the Appendix.

The full linear beam transport equation of one cavity equipped with couplers can then be written as

$$\vec{u}_1 = D_0\cdot\vec{k}_{\mathrm{down}}\left(D_1\cdot M_{\mathrm{RF}}\cdot D_1\cdot\vec{k}_{\mathrm{up}}\left(D_0\cdot\vec{u}_0\right)\right) \quad (22)$$

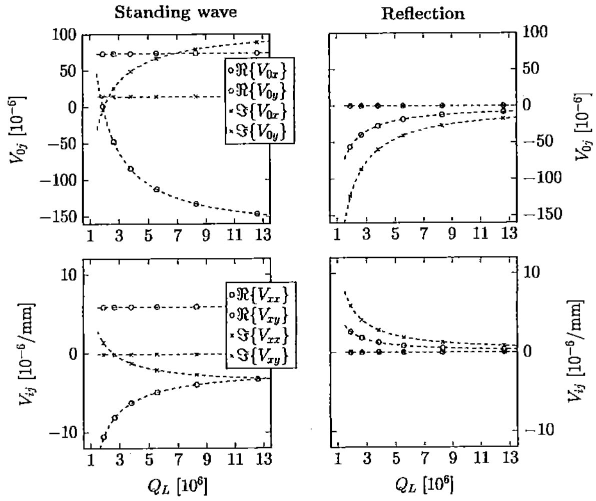

Figure 8. Normalized complex kick coefficients $[V_{0x}, V_{0y}, V_{xx}, V_{xy}]$ for the downstream coupler region as calculated via Eq. (16) with different field maps, reflecting different loaded quality factors Q_L. Plotted are the values related to the standing wave (left) and the reflection dependent part (right). The values are listed in Tables II and III.

where D_0 is the drift matrix from the reference positions to the coupler positions, respectively, D_1 the drift matrix between the couplers and the cavity and M_{RF} the axially symmetrical cavity transfer matrix. $\vec{k}_{\mathrm{up}}(\vec{u})$ and $\vec{k}_{\mathrm{down}}(\vec{u})$ evaluate the normalized upstream and downstream coupler kick, respectively, at the transverse coordinate $\vec{u} = [x, x', y, y']$, such that $\vec{k}(\vec{u}) = [x, x' + k_x(x,y), y, y' + k_y(x,y)]$. For the drift D_1 we use $d_1 = 3.54\,\mathrm{cm}$, while the cavity length is assumed to be $l_{\mathrm{cav}} = 9/2\lambda_{RF} = 1.0377\,\mathrm{m}$.

Figure 9 shows as an example the beam transport through one TESLA cavity as obtained by ASTRA and by the above described model in blue and red, respectively. Plotted are the horizontal (left) and vertical (right) positions (upper row) and momenta (lower row), as a function of the longitudinal coordinate z. The cavity is centered at $z = 0\,\mathrm{m}$ and the particle energy is increased from 10 MeV to 24 MeV.

The coloured bars in the lower row of Figure 9 illustrate the regions at which the different transfer matrices in Eq. (22) are applied. The red bar reflects the beam transport via the axially symmetrical RF cavity matrix M_{RF}, the yellow bar corresponds to the drift space D_1 between the cavity and the couplers and the black line to the drift D_0 between the couplers and the reference positions.

In this example, both the coupler kicks and the RF focusing are sufficiently well described by the linear beam dynamics model. However, a strong dependence of the model accuracy on the beam energy is expected, since the derivation of Eqs. (24, 17) uses the paraxial, thus

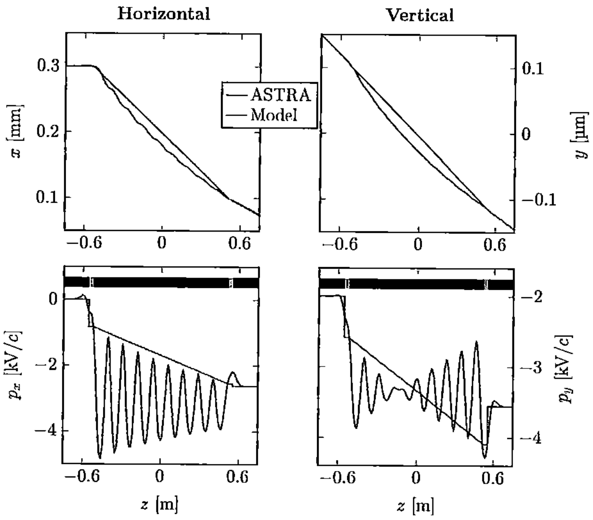

Figure 9. Particle trajectory through a TESLA cavity as calculated by ASTRA (blue) and the linear beam dynamics model (red, cf. Eq. (22)). Plotted are the horizontal (left) and vertical (right) positions (upper row) and momenta (lower row), respectively, as a function of the longitudinal coordinate z. The cavity is centered at $z = 0\,\mathrm{m}$. The coloured bars in the lower plots illustrate the different transfer matrices of the model. The red bar reflects the beam transport via the RF cavity matrix, the yellow bar corresponds to the drift space between the cavity and the couplers and the black line to the drift between the couplers and the reference positions. Beam initial and final energy is 10 MeV and 24 MeV, respectively.

ultra-relativistic assumption.

The accuracy of the linear beam dynamics model of Eq. (22) for different initial beam energies is calculated as follows. At each energy E_i, nine different RF phases between $\phi_{\mathrm{lim}} = \pm 20\,°$ and 7 different RF amplitudes between $V_{\mathrm{lim}} = [5\,\mathrm{MV\,m^{-1}}, 25\,\mathrm{MV\,m^{-1}}]$ are evaluated. At each step $[E, \phi, V]_i$, 10^4 particles with a Gaussian distribution of initial values $[x, p_x, y, p_y]_0$ with $\sigma_{x,y} = 2\,\mathrm{mm}$ and $\sigma_{p_x,p_y} = 5\,\mathrm{keV/c}$, respectively, are created. For each particle, the output of ASTRA is compared to the corresponding output of Eq. (22).

Results are shown in Figure 10. Plotted are the rms differences $[\Delta x, \Delta x', \Delta y, \Delta y']_{\mathrm{rms}}$, evaluated for all particles and RF amplitudes and phases, respectively, as a function of the initial beam energy E.

For beam energies in the order of some MeV the rms difference for one cavity may reach, for example, several 100 µm. The presented model is therefore rather unsuitable for accurate beam dynamics calculations regarding a TESLA based injector module as found at FLASH and European XFEL.

Above 100(10) MeV, however, the rms difference is well below 0.1 µm and 0.1 µrad, respectively, and the beam transport is sufficiently described by Eq. (22).

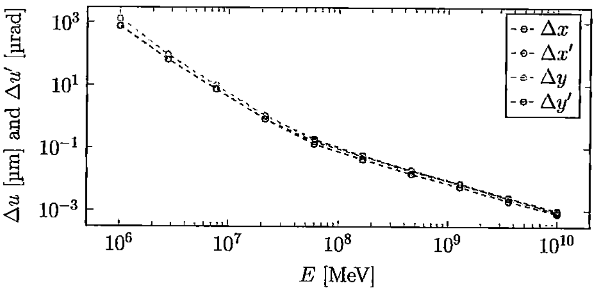

Figure 10. Comparison between the linear beam dynamics model (cf. Eq. (22)) and ASTRA for different initial beam energies E. Plotted are the rms differences $[\Delta x, \Delta x', \Delta y, \Delta y']_{\mathrm{rms}}$ as evaluated for 10^4 particles at different RF amplitudes and phases, respectively.

VII. EXPERIMENTAL VALIDATION OF DISCRETE COUPLER KICK MODEL

In this section the developed beam dynamics model is compared to dedicated experiments at FLASH and European XFEL.

A. Trajectory response measurements at European XFEL

Trajectory response measurements are a powerful diagnostic tool for linear accelerators [37]. In a linac, the (i, j)-th element of the trajectory response matrix is defined as the linearized response of a given coordinate (q_i) at the i-th monitor (BPM) to a kick Θ_j from the j-th steerer [38]

$$\Delta q_i = \left(R_{i \leftarrow j}\right)_{l,m} \cdot \Delta\Theta_j, \qquad (23)$$

with $R_{i\leftarrow j}$ being the beam transport matrix from point s_j to s_i. In the absence of coupling between the two transverse planes, the indices $l, m = 1, 2$ for the horizontal and $l, m = 3, 4$ for the vertical plane, respectively.

For a given set of RF parameters, the zeroth order coupler kick (cf. Eq. (17)), e.g. $k_x^0 \propto \Re\{V_{0x}\}$, reflects a constant kick on the bunch centroid. A trajectory response measurement is consequentially not affected. The first order kick $k_x^1 \propto \Re\{V_{xx} \cdot x + V_{xy} \cdot y\}$, however, depends on the transverse beam position in both planes. At sufficiently low beam energy, it is therefore expected that a trajectory response measurement disagrees considerably with an axially symmetrical beam dynamics model of a cavity and shows coupling between the two transverse planes.

The effect will be shown at the first main accelerating section of the European XFEL, of which a schematic drawing is shown in Figure 11. After the first bunch compressor (BC0), a linear accelerator (L1) increases the beam energy in four TESLA modules, thus 32 cavities,

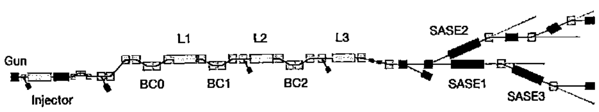

Figure 11. Schematic layout of the European XFEL (not to scale). The elements shown include 1.3 GHz (yellow) and 3.9 GHz (red) RF sections, undulators (green/red), main dipole magnets (blue), beam distribution systems (green) and beam dumps (black). The main accelerating sections (L1, L2, L3) contain 4, 12 and 84 accelerating modules, respectively.

from 150 MeV to 600 MeV. The optics server at European XFEL [39] currently uses ELEGANT [40] for the beam dynamics calculation of $R_{i\leftarrow j}$.

A trajectory response matrix is measured [41] and compared to the calculated response from the optics server. Additionally, the response is calculated with an optics model which includes discrete coupler kicks and calculates the beam transport through each cavity according to Eq. (22). The coupler kick coefficients have been interpolated according to Eq. (18) for $Q_L = 4 \times 10^6$.

Results are shown in Figure 12. Plotted are, as an example, the beam trajectories in both transverse planes as excited by an horizontal steerer at $s = 86$ m in the upper row. The lower row shows the corresponding trajectory response. The red marks indicate the measurements, whereas the black and blue lines reflect the calculated response both, by the default optic server and with the linear model including discrete coupler kicks. The position of the first cavity within the string of modules of about 50 m length is indicated by the vertical dotted line in the lower row.

Significant coupling from $x \to y$ occurs in the accelerating modules, which disagrees with the default optics model. A similar optics perturbation including transverse coupling has been also observed at the accelerating sections at FLASH [37, 38, 42].

The developed model including discrete coupler kicks is able to describe the observed coupling in both planes reasonably well. It can be concluded that the first order coupler kick is described sufficiently by the presented coupler kick model.

B. Coupler kick variations at FLASH

In this section coupler kick variations related to variations of the forward and backward traveling waves are studied experimentally at FLASH.

The Free-Electron Laser in Hamburg (FLASH) is a high-gain FEL user facility operating in the soft x-ray regime [2, 3]. The current layout of FLASH is shown in Figure 13. The RF setup at FLASH and its implication on transverse beam dynamics was studied in detail in Ref. [44]. Several cavities are supplied by one high power klystron in pulsed operation with a vector sum RF control. Within the RF flat top, long bunch trains

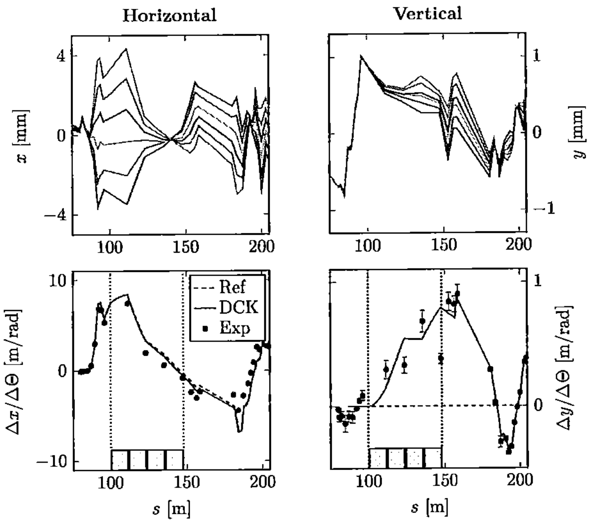

Figure 12. Trajectory response measurement at European XFEL. The upper row shows the horizontal (left) and vertical (right) beam trajectory as excited by an horizontal steerer at $s = 86$ m. The lower row shows the corresponding trajectory response as measured (red marks), and calculated both, by the default optic server (black) and with the linear model including discrete coupler kicks (DCK, blue, cf. Eq. (22)). The yellow rectangles in the lower row indicate the four accelerating modules of L1.

can be accelerated.

An experimental setup in which coupler kick variations within one bunch train can be isolated from the RF focusing at low beam energy was presented in Ref. [45] at the injector module at FLASH. In this section we present a similar experimental setup at high beam energy at the sixth accelerating module.

The cavity has a finite bandwidth. The cavity response to a modulation of the forward power is therefore limited. If the forward power is modulated with increasingly high frequencies Ω, the magnitude of the modulation of the accelerating field decreases with $\Delta V \propto 1/(1+i(\Omega+\Delta f)\tau)$ with τ being the decay time of the cavity. For very high modulation frequencies, the response of the accelerating field becomes negligible.

Regarding ultra-relativistic beams, transverse motion due to cavity off-axis fields is insignificant, since transverse magnetic and electric forces compensate each other

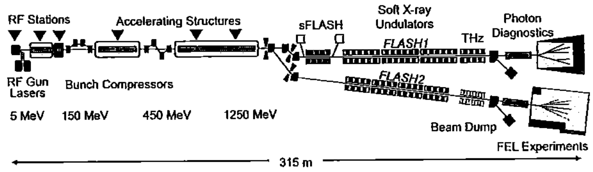

Figure 13. Schematic layout of the FLASH facility [43].

in axially symmetrical fields. Thus, coupler kick variations are expected to be the dominant source of transverse beam dynamics in this scenario.

The effect will be demonstrated at the sixth accelerating module (ACC6) at FLASH. The machine is set up with 400 bunches with a bunch repetition rate of 1 MHz. The RF signals of the forward and backward traveling waves for each cavity are measured. The RF data recorded in the data acquisition system [46] is manually recalibrated according to Ref. [47] in order to remove cross-coupling effects between the forward and backward signals. The beam trajectory is steered to be on axis through the modules and the position upstream and downstream ACC6 is measured.

The vector sum of ACC6 is $V_{\mathrm{VS}} = 62\,\mathrm{MV\,m^{-1}}$, the bunch charge 0.4 nC and initial beam energy is 600 MeV. The loaded quality factors of the eight cavities are measured as $[3.20, 3.11, 3.17, 3.12, 2.97, 3.02, 3.09, 3.05] \times 10^6$. Each measurement of BPM and RF data is an average over about 100 consecutive bunch trains with 10 Hz repetition rate to deal with short term jitter.

A reference is measured. Subsequently, the forward power within one bunch train is modulated with different frequencies.

The relative difference of the vector sum of the accelerating gradient δV_{VS} and the parameter $\Delta\mathbf{\Gamma}$ with respect to the reference setup is plotted in Figure 14. The modulation frequencies are 20 kHz, 50 kHz, 100 kHz and 300 kHz. For high modulation frequencies the variation of the accelerating field becomes small compared to the variation of $\mathbf{\Gamma}$.

In a second step the impact of coupler kick variations on the beam is studied. The measured beam position at the entrance of ACC6, initial beam energy and the RF signals are used to calculate the beam transport through the module. The beam transport for each bunch is evaluated using Eqs. (16, 17, 18, 22) iteratively for each cavity. The measured beam offset at the BPM downstream the last cavity is compared to the corresponding output of the model function.

Results are shown in Figure 15. Plotted are the differences of the horizontal and vertical BPM readouts between the modulated setup and the reference setup and the difference of the equivalent output of the model function. The negligible signal in the vertical plane even for low modulation frequencies points out that the beam dynamics at high beam energy and close to the cavity axis is dominated by the variation coupler kicks.

It can be concluded that the presented coupler kick model is both qualitatively and quantitatively able to reproduce the experimentally generated coupler kick variations.

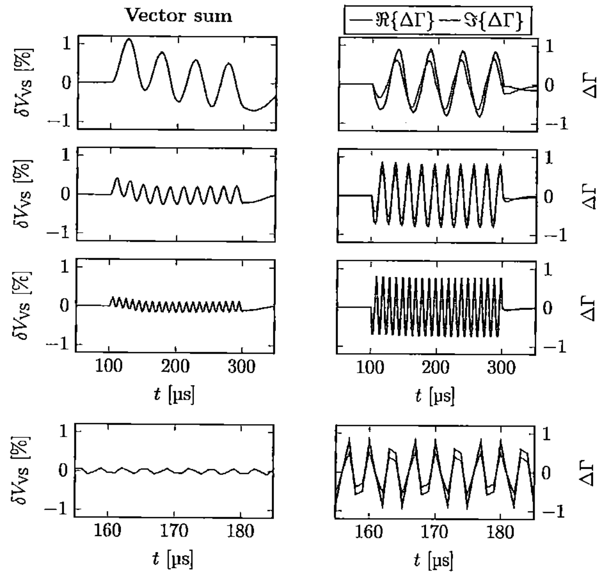

Figure 14. Variation of the vector sum of the accelerating gradient δV_{VS} (left) and the parameter $\Delta\mathbf{\Gamma}$ (right) at ACC6 at FLASH while applying modulations with different frequencies on the forward power (from top to bottom: 20 kHz, 50 kHz, 100 kHz and 300 kHz). The RF sampling time is 1 µs.

VIII. EXPECTED COUPLER KICK VARIATIONS AT EUROPEAN XFEL

In this section we investigate the influence of detuning related coupler kick variations on intra-bunch-train trajectory variations at the European XFEL [4–6].

The European XFEL main accelerator consists of 800 ILC style TESLA cavities, operated in pulsed mode with an RF flat top of 700 µs. The long RF pulse structure allows to provide long bunch-trains for the experiments.

The principles of RF induced intra-bunch-train trajectory variations have been described in detail in Ref. [44]. At European XFEL, several cavities with individual operational limits [48] are supplied by one RF power source. The low-level-RF system (LLRF) [20, 49] is able to restrict the variation of the vector sum of the amplitude and phase of the accelerating field below 0.01 % and 0.01 °, respectively [50]. However, caused by the effects of beam loading and Lorentz force detuning, individual cavities have an intrinsic variation of RF parameters within one bunch train. Misaligned cavities in combination with variable RF parameters induce intra-bunch-train trajectory variations.

The variation of the amplitude of the accelerating field within one bunch train, ΔV, is key in the creation of trajectory variations. For typical machine operation at European XFEL, the amplitude variation is determined mainly by the interaction of a common loaded quality factor Q_L with different operational gradients of the cavities [51]. LLRF simulations show that the beam loading

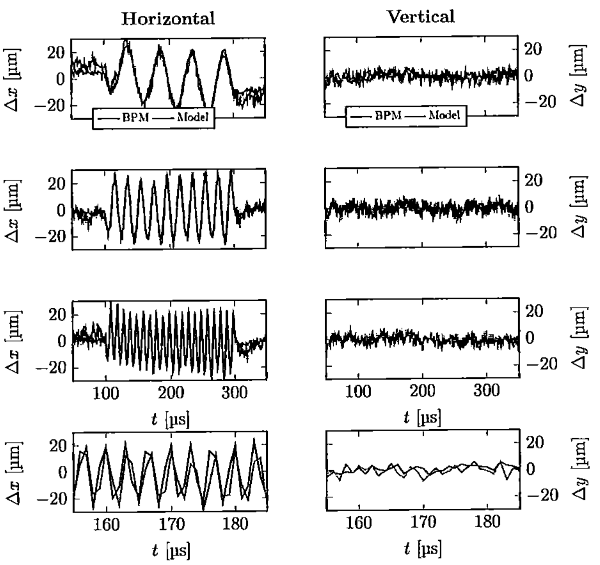

Figure 15. Experimental observation of intra bunch train coupler kick variations at ACC6 at FLASH. Plotted is the difference between the reference trajectories and the particle trajectories while applying modulations with different frequencies on the forward power (from top to bottom: 20 kHz, 50 kHz, 100 kHz and 300 kHz, cf Fig. 14). The bunch spacing is 1 µs. The BPM readout differences (black) and the corresponding model evaluations (colored) are plotted for the horizontal (left) and vertical (right) plane at the exit of the module.

induced amplitude variation is proportional to the beam current and can reach up to $4\,\mathrm{MV\,m^{-1}}$ for the design beam current of 4.5 mA and the actual spread in operational gradients [48] without further Q_L-correction.

Besides, additional beam dynamics perturbations regarding coupler kick variations have to be considered. High electromagnetic fields in resonators lead to strong Lorentz forces on the walls of these structures. In order to ensure the cooling, the thickness and therefore rigidness of the walls cannot be chosen freely. As a consequence, in a pulsed operation mode, the cavities are deformed dynamically in the range of some µm [20]. This results in a dynamic behavior of the resonance frequency, a Lorentz force detuning (LFD), which scales quadratically with the accelerating field. Due to the high Q_L, the LFD within one bunch train is comparable to the bandwidth of the cavity of about 300 Hz [52]. In order to compensate LFD at European XFEL, fine tuning for each cavity will be handled by double piezoelectric elements [53]. The residual intra-bunch-train detuning of individual cavities is dominated by microphonics and expected to be below 30 Hz.

The European XFEL linear accelerator increases the electron beam energy from 150 MeV to 17.5 GeV in 100 accelerating modules, thus an energy range in which the ultra-relativistic assumption is reasonable. In order to simulate the effect of trajectory jitter caused by detuning-related coupler kick variations, we use the developed beam dynamics model according to Eq. (22). The coupler kick coefficients for $Q_L = 4.6 \times 10^6$ are listed in Tables I, II and III. With the RF parameters obtained by Eqs. (25), the transfer matrices and coupler kick coefficients are calculated for each bunch and each cavity individually. Misalignments are modeled by coordinate transformations. A quadrupole magnet ($k = 0.0642\,\mathrm{m^{-1}}$) is located at the downstream end of each module, providing a FODO lattice in the accelerating sections. This is a model from the entrance of L1 to the end of L3 (cf. Fig. 11) with simplified optics.

As a figure of merit we use the final normalized trajectory variation $\Delta\tilde{u} = \sqrt{\beta_{u,f}\,(\gamma_{u,z}\,\Delta u_z^2 + 2\alpha_{u,z}\,\Delta u_z \Delta u_z' + \beta_{u,z}\,\Delta u_z'^2)}$, with $\alpha_{u,z}$ and $\beta_{u,z}$ being the Courant-Snyder parameters at position z and $\beta_{u,f}$ the beta function at the observation point, while u stands for the x and y axis. Casually speaking, $\Delta\tilde{u}$ measures the maximum observable offset variation at a point with a beta function of $\beta_{u,f}$ and zero divergence. For the upcoming analysis we will use $\beta_{x,f} = \beta_{y,f} = 30\,\mathrm{m}$, which reflects the design lattice at the intra-bunch-train transverse feedback system [54] downstream the accelerating sections.

For each machine seed the following model parameters are randomly created: variation of the amplitude ΔV and phase $\Delta\phi$ of the accelerating field and the detuning Δf of individual cavities within the bunch train, and the offset $\Delta u_{\mathrm{cav/mod}}$ and tilt $\Delta u'_{\mathrm{cav/mod}}$ of cavities and modules, respectively. For the range of misalignments we use $\Delta u_{\mathrm{cav/mod}} = \pm 0.5\,\mathrm{mm}$, $\Delta u'_{\mathrm{cav}} = \pm 0.3\,\mathrm{mrad}$ and $\Delta u'_{\mathrm{mod}} = \pm 0.2\,\mathrm{mrad}$.

The range of the intra-bunch-train variation of the RF parameters of individual cavities is increased subsequently. Maximum amplitude and phase variation are considered to be correlated as $\Delta\phi_{\max} = 2\,^\circ\,\mathrm{MV^{-1}\,m} \cdot \Delta V_{\max}$. For example, a maximum amplitude variation of $\Delta V_{\max} = 4\,\mathrm{MV\,m^{-1}}$ corresponds to a maximum variation of phase $\Delta\phi_{\max} = 8°$. This ratio is found to be reasonable for regular machine operation. At each parameter step $[\Delta V_{\max}, \Delta f_{\max}]_i$, 10^4 random machine seeds are created and the previously described beam transport model is evaluated.

Results are shown in Figure 16. The left side shows the rms value of the normalized trajectory variation $\Delta\tilde{u}_{\mathrm{rms}}$ at the end of the accelerator as a function of the maximum amplitude variation $\Delta V_{\max}$, evaluated for both planes and three detuning scenarios. The blue and red color correspond to horizontal and vertical plane, respectively, while the different plot marks reflect different detuning limits. The right plot shows $\Delta\tilde{u}_{\mathrm{rms}}$ for zero amplitude variation as a function of the maximum detuning $\Delta f_{\max}$.

For small amplitude variations the intra bunch train trajectory variation is dominated by detuning related coupler kick variations and trajectory variations occur mainly in the horizontal plane. For high amplitude variations the trajectory variation is proportional to the am-

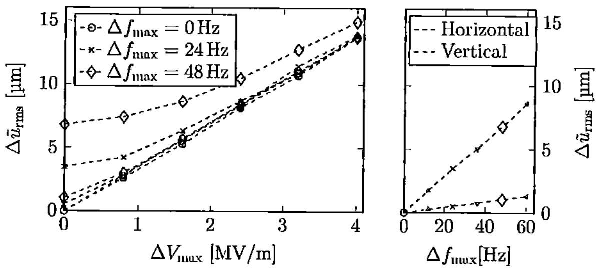

Figure 16. Normalized rms intra-bunch-train trajectory variation $\Delta\tilde{u}_{\rm rms}$ downstream the European XFEL accelerator as a function of the maximum variation of the amplitude of the accelerating field $\Delta V_{\rm max}$ (left) for the horizontal (blue) and vertical (red) plane. The different plot marks correspond to different maximum detuning $\Delta f_{\rm max}$. The right plot shows the trajectory variation for zero amplitude variation as a function of $\Delta f_{\rm max}$.

plitude variation, and the influence of detuning related coupler kick variations decreases.

It can be concluded that coupler kick variations are expected to be a minor concern in multibunch FEL operation at European XFEL. However, for high beam currents, a limitation of beam loading induced amplitude slopes by changing the Q_L-setup is advised.

IX. SUMMARY

Couplers break the axial symmetry of the TESLA cavities and affect the transverse beam dynamics considerably. The concept of first order discrete coupler kicks was presented, including a novel approach to separate the influence of the standing wave from the reflection dependent part. The developed beam dynamics model was compared to start to end tracking and dedicated experiments. Transverse coupling and detuning related coupler kick variations were described convincingly well. Numerical studies regarding European XFEL showed that detuning related coupler kick variations are expected to be a minor concern in regular operation.

X. ACKNOWLEDGMENTS

We would like to thank Igor Zagorodnov, Klaus Flöttmann and Ángel Ferran Pousa for proofreading and valuable comments. We wish to extend our particular thanks and appreciation to Wolfgang Ackermann, who with great skill and patience calculated the required field maps.

XI. APPENDIX

A. Cavity transfer matrix

The beam transport in an axial symmetric RF cavity can be written as $\vec{u} = M_{\rm RZ}\cdot\vec{u}_0$ with $\vec{u} = [u, u']$. The matrix elements R_{ij} of the transfer matrix of an axial symmetric cavity are given by Ref. [36] as

$$\begin{aligned}
R_{11} &= \cos\alpha - \sqrt{2}\cos\phi\sin\alpha \\
R_{12} &= \sqrt{8}\frac{\gamma_0}{\gamma'}\cos\phi\sin\alpha \\
R_{21} &= -\frac{\gamma'}{\gamma}\left(\frac{\cos\phi}{\sqrt{2}} + \frac{1}{\sqrt{8}\cos\phi}\right)\sin\alpha \\
R_{22} &= \frac{\gamma_0}{\gamma}\left(\cos\alpha + \sqrt{2}\cos\phi\sin\alpha\right)
\end{aligned} \tag{24}$$

where $\alpha = \frac{1}{\sqrt{8}\cos\phi}\cdot\ln\left(\frac{\gamma}{\gamma_0}\right)$ and γ_0 and $\gamma = \gamma_0 + \gamma'$ are the initial and final Lorentz factors, respectively.

B. LLRF equations

In order to relate the cavity detuning to the ratio of the forward and backward traveling waves, we assume a superconducting cavity operating close to the steady state condition, nearly on crest, with beam loading and a detuning small compared to the resonance frequency. The cavity voltage $\mathbf{V}_0$, the forward- and backward wave $\mathbf{V}_f$ and $\mathbf{V}_b$ and the beam current $\mathbf{I}_b$ are then related as [20]

$$\begin{aligned}
\mathbf{V}_0 &= \frac{1 + i\tan\psi}{1+\tan^2\psi}\cdot[2\,\mathbf{V}_f + R_L\cdot\mathbf{I}_B] \\
\mathbf{V}_0 &= \mathbf{V}_f + \mathbf{V}_b\,,
\end{aligned} \tag{25}$$

where the bold letters indicate complex numbers, for example $\mathbf{V}_0 = V_0\cdot e^{i\phi_0}$.

$\mathbf{I}_B$ is the complex beam current, which is $-2\,I_{B0}\,e^{i\phi_{\rm B}}$ where I_{B0} is the dc beam current and $\phi_{\rm B}$ describes the phase shift of the bunch with respect to a reference time. The shunt impedance R_L of a cavity without internal losses is determined by the product $Q_{\rm ext}(R/Q)$ with $Q_{\rm ext}$ being the external quality factor and (R/Q) being the ratio $V_0^2/(2\,W\,\omega_0)$ of the cavity voltage to the stored field energy W and frequency ω_0. The parameter (R/Q) depends only on the shape of a cavity.

The detuning angle ψ is defined as $\tan\psi = 2Q_L\Delta f/f_0$, with Δf being the detuning and f_0 the resonance frequency of the cavity. Using Equations (25) and assuming a constant beam current, the forward and backward wave can be expressed as a function of the phase difference ϕ_0 between the bunch and the cavity voltage with an amplitude of V_0 and the detuning $\Delta f = f_0 - f$. The parameter $\mathbf{\Gamma}$ follows as

$$\mathbf{\Gamma} = \frac{\mathbf{V}_b - \mathbf{V}_f}{\mathbf{V}_b + \mathbf{V}_f} = \frac{R_L\,\mathbf{I}_B}{\mathbf{V}_0} + i\frac{2\,Q_L}{f_0}\Delta f \tag{26}$$

C. Coupler kick coefficients

[1] Zhirong Huang and Kwang-Je Kim, "*Review of x-ray free-electron laser theory*," Phys. Rev. ST Accel. Beams **10**, 034801 (2007).

[2] Wolfgang Ackermann *et al.*, "Operation of a free-electron laser from the extreme ultraviolet to the water window," Nat Photon **1**, 336–342 (2007).

[3] B. Faatz *et al.*, "Simultaneous operation of two soft x-ray free-electron lasers driven by one linear accelerator," New J. Phys. **18**, 062002 (2016).

[4] R. Abela *et al.*, *XFEL: The European X-Ray Free-Electron Laser - Technical Design Report* (DESY, Hamburg, 2006) pp. 1–646.

[5] Winfried Decking and Torsten Limberg, European XFEL Post-TDR Description, Tech. Rep. XFEL.EU TN-2013-004 (2013).

[6] T. Tschentscher, Layout of the X-Ray Systems at the European XFEL, Tech. Rep. XFEL.EU TR-2011-001 (2011).

[7] B. Aune, R. Bandelmann, D. Bloess, B. Bonin, A. Bosotti, M. Champion, C. Crawford, G. Deppe, B. Dwersteg, D. A. Edwards, H. T. Edwards, M. Ferrario, M. Fouaidy, P.-D. Gall, A. Gamp, A. Gössel, J. Graber, D. Hubert, M. Hüning, M. Juillard, T. Junquera, H. Kaiser, G. Kreps, M. Kuchnir, R. Lange, M. Leenen, M. Liepe, L. Lilje, A. Matheisen, W.-D. Möller, A. Mosnier, H. Padamsee, C. Pagani, M. Pekeler, H.-B. Peters, O. Peters, D. Proch, K. Rehlich, D. Reschke, H. Safa, T. Schilcher, P. Schmüser, J. Sekutowicz, S. Simrock, W. Singer, M. Tigner, D. Trines, K. Twarowski, G. Weichert, J. Weisend, J. Wojtkiewicz, S. Wolff, and K. Zapfe, "Superconducting tesla cavities," Phys. Rev. ST Accel. Beams **3**, 092001 (2000).

[8] J. Sekutowicz, "Higher order mode coupler for TESLA," in *Hamburg DESY - DESY TESLA 94-07 (94/02,rec.Mar.) 14 p* (1994).

[9] P. Piot *et al.*, "*Steering and Focusing Effects in TESLA Cavity Due to High Order Mode and Input Couplers*," in *Proceedings, PAC05, Knoxville, USA, 2005*, session ID: WPAT083 (JACoW, Geneva, Switzerland).

[10] Klaus Floettmann, "rf-induced beam dynamics in rf guns and accelerating cavities," Phys. Rev. ST Accel. Beams **18**, 064801 (2015).

[11] E. Prat, W. Decking, M. Dohlus, T. Limberg, and I. Zagorodnov, "*Impact of Electromagnetic Fields in TESLA RF Modules on Transverse Beam Dynamics*," in *Proceedings, EPAC08, Genoa, Italy, 2008*, Vol. C0806233 (JACoW, Geneva, Switzerland) p. 1568.

[12] M. Dohlus *et al.*, "*Numerical Investigations Of Waveguide Input Couplers For The TESLA Superstructure*," in *Proceedings, EPAC00, Vienna, Austria, 2000*, session ID: TUP5B03 (JACoW, Geneva, Switzerland).

[13] A. Vivoli *et al.* (LCLS-II), "Effect of Cavity Couplers Field on the Beam Dynamics of the LCLS-II Injector," in *Proceedings, 27th Linear Accelerator Conference, LINAC2014, Geneva, Switzerland, August 31-September 5, 2014* (JACoW, Geneva, Switzerland, 2014) p. THPP060.

[14] N. Juntong, Roger M. Jones, I. R. R. Shinton, C. D. Beard, and G. Burt, "RF Coupler Kicks and Wakefields in SC Accelerating Cavities," *Particle accelerator. Proceedings, 11th European Conference, EPAC 2008, Genoa, Italy, June 23-27, 2008*, Conf. Proc. **C0806233**, WEPP085 (2008).

[15] M. Dohlus, I. Zagorodnov, E. Gjonaj, and T. Weiland, "*Coupler Kick for Very Short Bunches and its Compensation*," in *Proceedings, EPAC08, Genoa, Italy, 2008*, session ID: MOPP013 (JACoW, Geneva, Switzerland) p. 582.

[16] Dirk Kruecker, I. Melzer-Pellmann, Dirk Poirier, F. Kruecker, I. Melzer-Pellmann, F. Poirier, and N. J. Walker, "*Simulation Studies on Coupler Wakefield and RF Kicks for the International Linear Collider with MERLIN*," in *Proceedings, EPAC08, Genoa, Italy, 2008*, Vol. C0806233 (JACoW, Geneva, Switzerland) p. TUPP047.

[17] N. Solyak, I. Gonin, A. Latina, A. Lunin, K. Ranjan, and V. Yakovlev, "RF kick in the ILC acceleration structure," *Particle accelerator. Proceedings, 11th European Conference, EPAC 2008, Genoa, Italy, June 23-27, 2008*, Conf. Proc. **C0806233**, MOPP042 (2008).

[18] Brandon Buckley and Georg H. Hoffstaetter, "Transverse emittance dilution due to coupler kicks in linear accelerators," Phys. Rev. ST Accel. Beams **10**, 111002 (2007).

[19] A. Saini *et al.*, "*Study of Coupler's Effects on ILC Like Lattice*," in *Proceedings, IPAC10, Kyoto, Japan, 2010*, session ID: THPD088 (JACoW, Geneva, Switzerland).

[20] T. Schilcher, Vector Sum control of pulsed accelerating fields in Lorentz Force Detuned Superconducting Cavities, Ph.D. thesis, University of Hamburg (1998).

[21] A. Neumann:, Compensating microphonics in SRF cavities to ensure beam stability for future free-electron-lasers, Ph.D. thesis, Humboldt-Universität zu Berlin (2008).

[22] N. Baboi, M. Dohlus, C. Magne, A. Mosnier, O. Napoly, and H. W. Glock, "Investigation of a high-Q dipole mode at the TESLA cavities," in *Particle accelerator. Proceedings, 7th European Conference, EPAC 2000, Vienna, Austria, June 26-30, 2000. Vol. 1-3* (JACoW, Geneva, Switzerland, 2000) pp. 1107–1119.

[23] N Baboi:, "*Multi-Bunch Beam Dynamics Studies for the European XFEL*," in *Proceedings, LINAC04, Luebeck, Germany, 2004*, session ID: TUP41 (JACoW, Geneva, Switzerland).

[24] B. Dwersteg, D. Kostin, M. Lalayan, C. Martens, and W.-D. Möller, "Tesla rf power couplers development at desy," in *10th Workshop on RF Superconductivity (SRF 2001) Tsukuba, Japan, September 6-11, 2001* (2001) pp. 443–447.

[25] Ties Behnke, James E. Brau, Brian Foster, Juan Fuster, Mike Harrison, James McEwan Paterson, Michael Peskin, Marcel Stanitzki, Nicholas Walker, and Hitoshi Yamamoto, "The International Linear Collider Technical Design Report - Volume 1: Executive Summary," DESY-13-062 (2013), arXiv:1306.6327 [physics.acc-ph].

Table I. Coupler kick coefficients of the upstream coupler for the standing wave, V_u^{SW} (1.3 GHz cavity) and corresponding upstream and downstream V_u^{SW}, V_d^{SW} and the downstream reflection dependent part, V_d^{R}, for the 3.9 GHz cavity (cf. Eq. (16)).

Type	V_{0x} $[10^{-6}]$	V_{0y} $[10^{-6}]$	V_{xx} $[10^{-6}\mathrm{mm}^{-1}]$	V_{xy} $[10^{-6}\mathrm{mm}^{-1}]$
1.3 GHz V_u^{SW}	$-113.98+19.25i$	$-82.10-0.47i$	$2.03-1.60i$	$6.81-0.73i$
3.9 GHz V_u^{SW}	$-190.95+497.18i$	$-59.89+286.52i$	$9.96-31.34i$	$11.36-48.34i$
3.9 GHz V_d^{SW}	$-1036.43-76.68i$	$62.03+253.47i$	$42.53-75.49i$	$10.96+46.73i$
3.9 GHz V_d^{R}	$-101.30+113.30i$	$7.46-2.11i$	$6.85-6.44i$	$1.25-0.58i$

Table II. Coupler kick coefficients of the downstream coupler for the standing wave, V_d^{SW} (cf. Eq. (16)), as calculated with different field maps of the 1.3 GHz cavity for different values of the loaded quality factor Q_L. The values for $Q_L = 3.1 \times 10^6$ and $Q_L = 4.6 \times 10^6$ reflect the standard Q_L-setting for FLASH and European XFEL, respectively, and are evaluated using Eq. (18) and the fit parameters listed in Table IV.

Q_L $[10^6]$	V_{0x} $[10^{-6}]$	V_{0y} $[10^{-6}]$	V_{xx} $[10^{-6}\mathrm{mm}^{-1}]$	V_{xy} $[10^{-6}\mathrm{mm}^{-1}]$
1.91	$1.03-3.55i$	$73.13+14.40i$	$-10.54+1.40i$	$5.85-0.13i$
2.67	$-47.47+25.92i$	$73.24+14.50i$	$-8.11-0.11i$	$5.85-0.14i$
3.10	$-61.43+34.60i$	$73.31+14.47i$	$-7.41-0.55i$	$5.85-0.14i$
3.81	$-84.39+48.87i$	$73.41+14.43i$	$-6.27-1.26i$	$5.86-0.14i$
4.60	$-97.03+56.79i$	$73.56+14.37i$	$-5.67-1.63i$	$5.87-0.13i$
5.57	$-112.59+66.53i$	$73.75+14.31i$	$-4.94-2.09i$	$5.88-0.10i$
8.30	$-132.71+79.46i$	$73.85+14.32i$	$-3.97-2.73i$	$5.88-0.13i$
12.61	$-146.59+88.52i$	$73.76+14.31i$	$-3.26-3.16i$	$5.91-0.06i$

Table III. Coupler kick coefficients of the downstream coupler for the reflection dependent part, V_d^{R} (cf. Eq. (16)), as calculated with different field maps of the 1.3 GHz cavity for different values of the loaded quality factor Q_L. The values for $Q_L = 3.1\times10^6$ and $Q_L = 4\times10^6$ reflect the standard Q_L-setting for FLASH and European XFEL, respectively, and are evaluated using Eq. (18) and the fit parameters listed in Table V.

Q_L $[10^6]$	V_{0x} $[10^{-6}]$	V_{0y} $[10^{-6}]$	V_{xx} $[10^{-6}\mathrm{mm}^{-1}]$	V_{xy} $[10^{-6}\mathrm{mm}^{-1}]$
1.91	$-56.13-123.56i$	$0.06+0.56i$	$2.61+5.89i$	$0.01+0.04i$
2.67	$-39.46-86.76i$	$0.06+0.39i$	$1.82+4.11i$	$0.00+0.03i$
3.10	$-34.84-76.57i$	$0.05+0.34i$	$1.61+3.62i$	$0.00+0.03i$
3.81	$-27.24-59.82i$	$0.04+0.25i$	$1.25+2.82i$	$0.00+0.02i$
4.60	$-23.29-51.14i$	$0.04+0.21i$	$1.07+2.41i$	$0.00+0.02i$
5.57	$-18.44-40.47i$	$0.04+0.16i$	$0.84+1.90i$	$0.00+0.01i$
8.30	$-12.28-26.89i$	$0.04+0.10i$	$0.56+1.26i$	$0.00+0.01i$
12.61	$-8.03-17.59i$	$0.03+0.06i$	$0.37+0.82i$	$0.00+0.01i$

Table IV. Fit parameters from Eq. (18) for downstream coupler kick coefficients for the standing wave, V_d^{SW}.

c_i	V_{0x}	V_{0y} $[10^{-6}]$	V_{xx} $[10^{-6}\mathrm{mm}^{-1}]$	V_{xy} $[10^{-6}\mathrm{mm}^{-1}]$
c_1	-174.132	74.052	-1.982	6.256
c_2	348.293	-2.629	-16.418	-23.199
c_3	0.080	0.836	0.010	55.048
c_4	106.447	14.161	-3.985	14.400
c_5	-229.199	2.425	10.533	0.000
c_6	0.175	6.404	0.048	0.000

Table V. Fit parameters from Eq. (18) for downstream coupler kick coefficients for the reflection dependent part, V_d^{R}.

c_i	V_{0x}	V_{0y} $[10^{-6}]$	V_{xx} $[10^{-6}\mathrm{mm}^{-1}]$	V_{xy} $[10^{-6}\mathrm{mm}^{-1}]$
c_1	0.039	0.018	-0.003	0.001
c_2	-100.876	0.149	4.588	0.009
c_3	-0.113	1.482	-0.155	0.132
c_4	0.153	-0.028	-0.006	-0.000
c_5	-221.462	1.057	10.327	0.073
c_6	-0.119	-0.106	-0.157	-0.196

[26] V. Katalev *et al.*, "*Tuning of External Q And Phase for The Cavities of A Superconducting Linear Accelerator*," in *Proceedings, LINAC04, Luebeck, Germany, 2004*, session ID: THP51 (JACoW, Geneva, Switzerland).

[27] B. Aune *et al.*, "*Superconducting TESLA cavities*," Phys. Rev. ST Accel. Beams **3**, 092001 (2000).

[28] J. Sekutowicz, R. Wanzenberg, and T. Weiland, "A design of a 3rd harmonic cavity for the ttf 2 photoinjector," in *Tesla-fel 2002-05* (JACoW, Geneva, Switzerland, 2002).

[29] N. Solyak, I. Gonin, H. Edwards, M. Foley, T. Khabiboulline, D. Mitchell, J. Reid, and L. Simmons, "Development of the third harmonic SC cavity at Fermilab," *Particle accelerator. Proceedings, Conference, PAC 2003, Portland, USA, May 12-16, 2003*, Conf. Proc. **C030512**, 1213 (2003).

[30] Elvin Harms, Helen Edwards, Markus Hüning, and Elmar Vogel, "Commissioning and Early Operating Experience of the FLASH Third Harmonic RF System," in *Proceedings, 25th International Linear Accelerator Conference, LINAC2010: Tsukuba, Japan, September 12-17, 2010* (JACoW, Geneva, Switzerland, 2011) p. TUP013.

[31] P. Pierini, M. Bertucci, A. Bosotti, C. Maiano, P. Michelato, L. Monaco, R. Paparella, D. Sertore, C. Pagani, and E. Vogel, "European XFEL 3.9 GHz System," 16th International Conference on RF Superconductivity, Paris (France), 23 Sep 2013 - 27 Sep 2013 (JACoW, Geneva, Switzerland, 2013) p. 3 p.

[32] Wolfgang Ackermann and Thomas Weiland, "*High Precision Cavity Simulations*," in *Proceedings, ICAP12, Rostock-Warnemünde, Germany, 2012*, session ID: MOADI1 (JACoW, Geneva, Switzerland).

[33] "Link to 3D field map of the TESLA cavity: `http://www.desy.de/fel-beam/s2e/data/TESLA/WA_original/`," (2017).

[34] "Link to 3D field map of the 3.9 GHz cavity: `http://www.desy.de/fel-beam/s2e/data/TESLA/WA_original/`," (2017).

[35] K. Flöttmann:, "*A Space Charge Tracking Algorithm - ASTRA*," (1997).

[36] E. E. Chambers:, "*Particle Motion in a Standing Wave Linear Accelerator*," in *1968 Summer Study on Superconducting Devices and Accelerators Brookhaven, New York, USA, 1968*, pp. 79–100.

[37] Thorsten Hellert, *Studies on orbit response matrices at the high-gain free electron laser FLASH*, Master's thesis, University of Hamburg (2012).

[38] Johann Zemella, Thorsten Hellert, Matthias Scholz, and Mathias Vogt, "Progress in Optics Studies at FLASH," in *Proceedings, 6th International Particle Accelerator Conference (IPAC 2015): Richmond, Virginia, USA, May 3-8, 2015* (JACoW, Geneva, Switzerland, 2015) p. TUPWA035.

[39] S. Meykopff, "An optics-suite and -server for the european xfel," in *Proceedings, PCaPAC14, Karlsruhe, Germany, 2014* (JACoW, Geneva, Switzerland) p. WPO009.

[40] M. Borland, "elegant: A flexible sdds-compliant code for accelerator simulation," Advanced Photon Source LS-287 (2000).

[41] Lars Froehlich, Christopher Behrens, Bolko Beutner, Maria-Elena Castro-Carballo, Winfried Decking, Olaf Hensler, Raimund Kammering, Torsten Limberg, Sascha Meykopff, Matthias Scholz, Jan Szczesny, Josef Wilgen, Enrico Allaria, and Giuseppe Penco, "High Level Software for the Commissioning of the European XFEL," 11th International Workshop on Personal Computers and Particle Accelerator Controls, Campinas (Brazil), 25 Oct 2016 - 28 Oct 2016 (JACoW, Geneva, Switzerland, 2016) p. 4.

[42] Johann Zemella, Thorsten Hellert, Matthias Scholz, and Mathias Vogt, "Measurements of the Optical Functions at FLASH," in *Proceedings, 5th International Particle Accelerator Conference (IPAC 2014): Dresden, Germany, June 15-20, 2014* (JACoW, Geneva, Switzerland, 2014) p. TUPRO050.

[43] FLASH webpage:, "`flash.desy.de`," (2016).

[44] Thorsten Hellert, Winfried Decking, and Julien Branlard, "Analysis of multibunch free electron laser operation," Phys. Rev. Accel. Beams **20**, 090702 (2017).

[45] Thorsten Hellert, Martin Dohlus, and Winfried Decking, "Efficient model for low-energy transverse beam dynamics in a nine-cell 1.3 ghz cavity," Phys. Rev. Accel. Beams **20**, 100702 (2017).

[46] V. Rybnikov *et al.*, "*Data acquisition system for a VUV-FEL linac*," in *Proceedings, PCaPAC05, Hayama, Japan, 2005*, p. WEB1.

[47] S. Pfeiffer *et al.*, "*Virtual Cavity Probe Generation using Calibrated Forward and Reflected Signals*," in *Proceedings, IPAC15, Richmond, Virginia, USA, 2015*, session ID: MOPWA040 (JACoW, Geneva, Switzerland).

[48] D. Reschke, V. Gubarev, J. Schaffran, L. Steder, N. Walker, M. Wenskat, and L. Monaco, "Performance in the vertical test of the 832 nine-cell 1.3 ghz cavities for the european x-ray free electron laser," Phys. Rev. Accel. Beams **20**, 042004 (2017).

[49] J. Branlard *et al.*, "The european xfel llrf system," in *Proceedings of the 3rd International Conference on Particle Accelerators, IPAC12, New Orleans, USA, 2012* (JACoW, Geneva, Switzerland) p. 55.

[50] C. Schmidt *et al.*, "*Operation Experiences with the MICROTCA.4-based LLRF Control System at FLASH*," in *Proceedings of the 6th International Particle Accelerator Conference, IPAC15, Richmond, Virginia, USA, 2015* (JACoW, Geneva, Switzerland, 2015) p. 844.

[51] Thorsten Hellert, Intra-Bunch-Train Transverse Dynamics in the Superconducting Accelerators FLASH and European XFEL, Ph.D. thesis, University of Hamburg (2017).

[52] C. Schmidt, RF system modeling and controller design for the European XFEL, Ph.D. thesis, University of Hamburg (2010).

[53] Konrad Przygoda, Julien Branlard, Wojciech Cichalewski, Olaf Hensler, Karol Kasprzak, Tomasz Poźniak, Holger Schlarb, and Christian Schmidt, "*Testing Procedures for Fast Frequency Tuners of XFEL Cavities*," in *Proceedings of the 6th International Particle Accelerator Conference, IPAC15, Richmond, Virginia, USA, 2015* (JACoW, Geneva, Switzerland) p. 2991.

[54] B. Keil *et al.*, "Status of The European XFEL Transverse Intra Bunch Train Feedback System," in *Proceedings, IBIC15, Melbourne, Australia, 2015*, session ID: TUPB064 (JACoW, Geneva, Switzerland).